RAA 2016 Vol. **16** No. **11**, 165 (6pp) doi: 10.1088/1674–4527/16/11/165

http://www.raa-journal.org *http://iopscience.iop.org/raa*

***R**esearch in*
***A**stronomy and*
***A**strophysics*

Acceleration feedback of a current-following synchronized control algorithm for telescope elevation axis

Tao Tang[1,2], Tong Zhang[1,2], Jun-Feng Du[1,2], Ge Ren[1,2] and Jing Tian[1,2,3]

[1] Key Laboratory of Optical Engineering, Chinese Academy of Sciences, Chengdu 610209, China; *tangtao24@163.com*
[2] The Institute of Optics and Electronics, Chinese Academy of Sciences, Chengdu 610209, China
[3] School of Opto-Electronic Information, University of Electronic Science and Technology of China, Chengdu 610054, China

Received 2016 May 4; accepted 2016 June 3

Abstract This paper proposes a dual-motor configuration to enhance closed-loop performance of a telescope control system. Two identical motors are mounted on each side of a U-type frame to drive the telescope elevation axis instead of a single motor drive, which is usually used in a classical design. This new configuration and mechanism can reduce the motor to half the size used in the former design, and it also provides some other advantages. A master-slave current control mode is employed to synchronize the two motors. Acceleration feedback control is utilized to further enhance the servo performance. Extensive experiments are used to validate the effectiveness of the proposed control algorithm in synchronization, disturbance attenuation and low-velocity tracking.

Key words: telescopes — instrumentation: control method — instrumentation miscellaneous: high angular resolution — instrumentation: detector — control software

1 INTRODUCTION

A large telescope (Rao et al. 2014) is usually efficient in the field of space observation. However, there are some challenges in optical configurations, mechanical systems, the primary mirror, thermal control, control systems and other issues (MacMartin 2003; Gawronski 2007). This paper focuses on the elevation axis control system of a telescope. A single motor is usually used to drive the telescope, which causes the U-type mechanical frame (Rao et al. 2014) to deform due to the heavy lens tube and wide span. A dual-motor configuration of the direct drive control system is proposed to drive the elevation axis. This configuration and mechanism are expected to reduce the size of the single motor mechanism by half while still providing equivalent torque and decreased mechanical deformation. Synchronized control of the two motors has thus become a fundamental problem. Several classical control methods for synchronous drive are provided in the existing literature (Perez-Pinal et al. 2004; Pérez-Pinal et al. 2005). In this paper, an acceleration feedback control (AFC) algorithm (Andersen & Zurbuchen 1976; Higginson et al. 1991) based on master-slave current controls is employed to enhance the high closed-loop performance. AFC has been experimentally validated in several precision control systems (Sedghi et al. 2008; Xu et al. 2000). As a popular example, the 3.6 m ESO telescope can work well with AFC compensating mechanical resonances (Andersen & Zurbuchen 1976). The remainder of this paper is organized as follows. Section 2 presents a detailed introduction to the dual-motor configuration and model. Section 3 focuses on implementation of the control loops, such as current loop, acceleration loop and velocity loop. Section 4 sets up experiments to validate the control system. Concluding remarks are presented in Section 5.

2 DUAL-MOTOR CONTROL MODEL

Many telescopes have a U-type mechanical frame (Rao et al. 2014) to support the lens tube as shown in Figure 1. This paper introduces a dual-motor configuration, with two identical motors on each side of the U-type frame, which is different from previous designs that only had a single motor on either the left side or right side of the U-type frame. The power provided by a motor is proportional to its diameter. Therefore, it is reasonable to replace a single motor with two identical motors that have half the diameter.

If the optical tube assembly is driven by a single motor, the left motor is chosen as the actuator because of symmetry of the mechanical configuration. The dynamical equations are set up according to Newton's laws of motion

$$J_1\ddot{\theta}_1 + K_1(\theta_1 - \theta_{\rm Lo}) = \tau_1, \quad (1)$$

$$J_{\rm Lo}\ddot{\theta}_{\rm Lo} + K_1(\theta_{\rm Lo} - \theta_1) = 0. \quad (2)$$

We can provide theoretical analysis, even though Equations (1) and (2) only approximately describe the con-

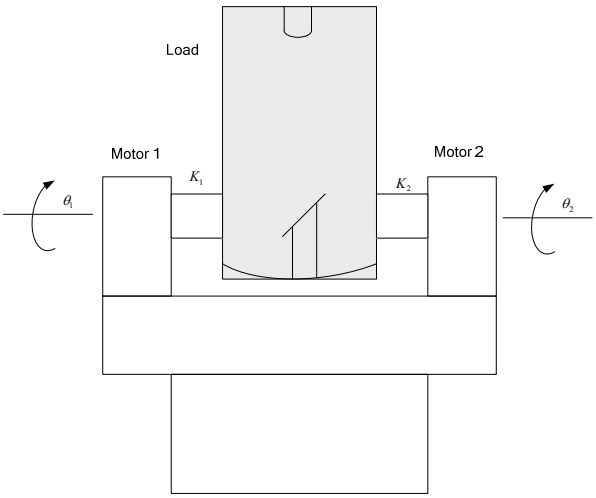

Fig. 1 Dual-motor configuration of telescope elevation axis.

trol system roughly due to a shortage of high-frequency signals. In fact, a complicatedly high-order model can be reduced using some methods (Ding et al. 2016, 2015). From Equations (1) and (2), the transfer function from $\dot{\theta}_1$ to τ_1 (the velocity open-loop frequency response) is obtained as follows

$$\frac{\dot{\theta}_1}{\tau_1} = \frac{1}{s(J_1 + J_{\rm Lo})} \frac{J_{\rm Lo}s^2 + K_1}{\frac{J_1 J_{\rm Lo} s^2}{(J_1 + J_{\rm Lo})} + K_1}. \quad (3)$$

The frequencies of the main resonance and anti-resonance are

$$\omega_r = \sqrt{\frac{K_1(J_1 + J_{\rm Lo})}{J_1 J_{\rm Lo}}} \approx \sqrt{\frac{K_1}{J_1}}, \quad \omega_{\rm ar} = \sqrt{\frac{K_1}{J_{\rm Lo}}}. \quad (4)$$

To distinguish the dual-motor case from the single-motor case, J_1' is introduced to replace J_1 and is defined as the moment of inertia for the left motor in the dual-motor configuration Other parameters denoted with a prime symbol ($'$) correspond to the single-motor configuration in this paper. The dynamical equations are also established as follows.

$$J_1'\ddot{\theta}'_1 + K_1'(\theta_1' - \theta_{\rm Lo}) = \tau_1', \quad (5)$$

$$J_{\rm Lo}\ddot{\theta}'_{\rm Lo} + K_1'(\theta_{\rm Lo} - \theta_1') + +K_2'(\theta_{\rm Lo} - \theta_2') = 0, \quad (6)$$

$$J_2'\ddot{\theta}'_2 + K_2'(\theta_2' - \theta_{\rm Lo}) = \tau_2'. \quad (7)$$

Suppose $\tau_1' = \tau_2' = 0.5\tau_1$, $J_1' = J_2' = 0.5J_1$, $K_1' = K_2'$. Let $\tau = \tau_1' + \tau_2'$, then

$$\frac{\dot{\theta}'_1}{\tau_1} = \frac{1}{s} \frac{J_{\rm Lo}s^2 + 2K_1'}{J_2' J_{\rm Lo} s^2 + (2J_2' + J_{\rm Lo})s^2} + K_1', \quad (8)$$

$$\omega_r' = \sqrt{\frac{K_1'(J_2' + J_{\rm Lo})}{J_2' J_{\rm Lo}}} \approx \sqrt{\frac{K_1'}{J_2'}}, \quad \omega_{\rm ar}' = \sqrt{\frac{2K_1'}{J_{\rm Lo}}}. \quad (9)$$

Comparing Equation (4) with Equation (9), the anti-resonance frequency in a dual-motor system becomes $\sqrt{2}$ times more than that with a single motor drive, but their primary resonance frequencies are nearly identical.

The open-loop frequency response of the velocity is provided in Figure 2. The primary anti-resonance frequency with a dual-motor is about 80 Hz, but it is approximately 60 Hz in a single motor drive system. Their resonance frequencies are located at a frequency of 350 Hz. Noting that the open-loop response below 40 Hz is closer to 1/S than that with a single motor, the dual-motor drive system can facilitate reducing the friction torque and inertial delay in the symmetric configuration.

3 IMPLEMENTATIONS OF THE CONTROL SCHEME

A current-following control mode instead of a master-slave speed control mode (Perez-Pinal et al. 2004; Pérez-Pinal et al. 2005) is employed to drive the load to respond synchronously and quickly. The dashed box in Figure 3 represents the current feedback loop. The sign $i_{\rm in}$ is the input of the current loop; at the same time, it is also the output of the acceleration loop. The sign $i_{\rm out}$ is the output of the current loop. It is practical to implement a bandwidth of several hundred Hertz for the current closed-loop response (Xu et al. 2000) because this value is not limited by mechanical resonances. The loop outside the current loop is the acceleration loop, which only has a bandwidth of several tens of Hertz, and is mainly constrained by mechanical vibrations. The acceleration loop can simplify the open-loop response of the velocity similar to an integrator term below the bandwidth of the closed-loop response for acceleration. The proposed control structure is shown in Figure 3.

3.1 Current Loop

The armature current of the motor can be measured by a Hall current sensor and it can serve as the feedback signal. A classic PI-type controller (Xu et al. 2000) is available to realize the current closed-loop control. The transfer func-

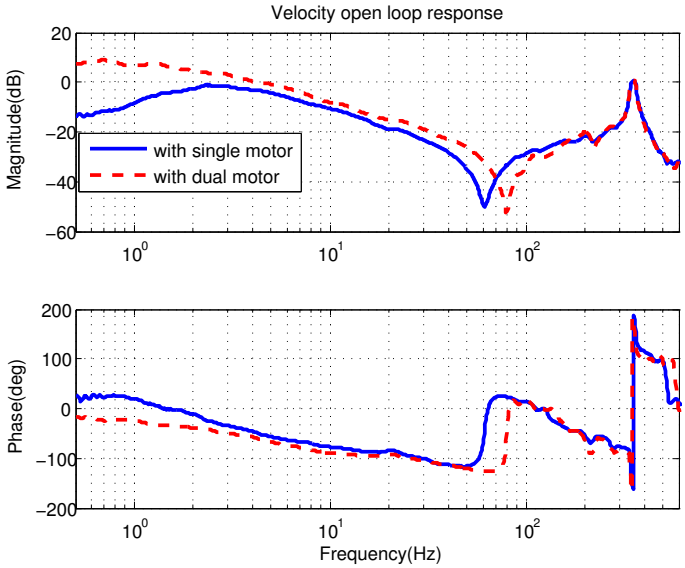

Fig. 2 Velocity open-loop frequency response.

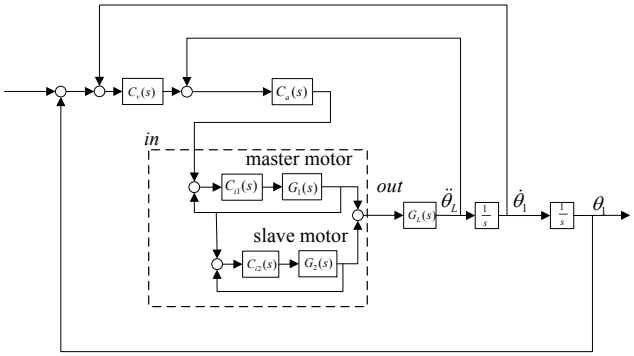

Fig. 3 Control scheme with dual motors.

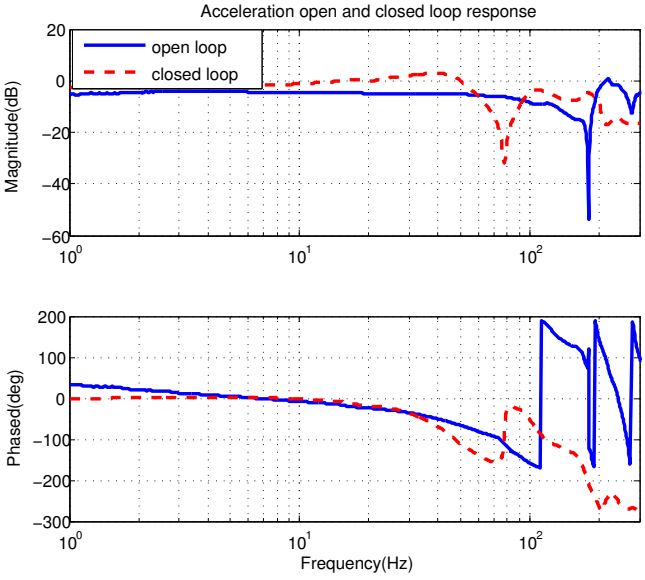

Fig. 4 Acceleration loop frequency response.

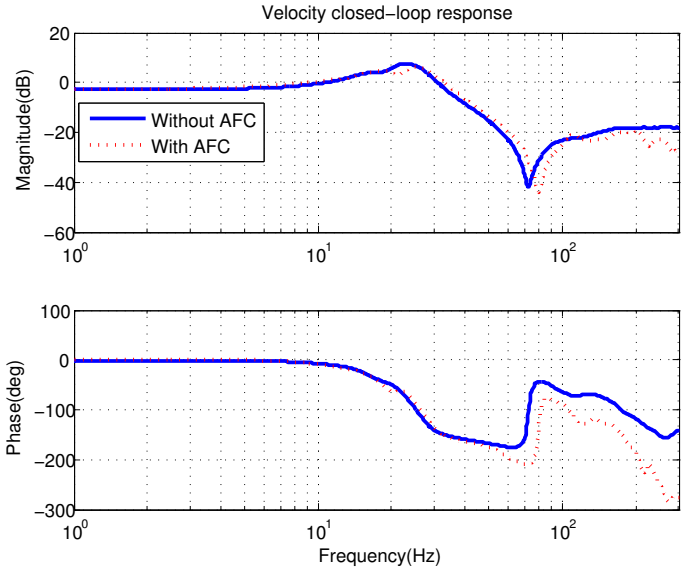

Fig. 5 Velocity closed-loop frequency response.

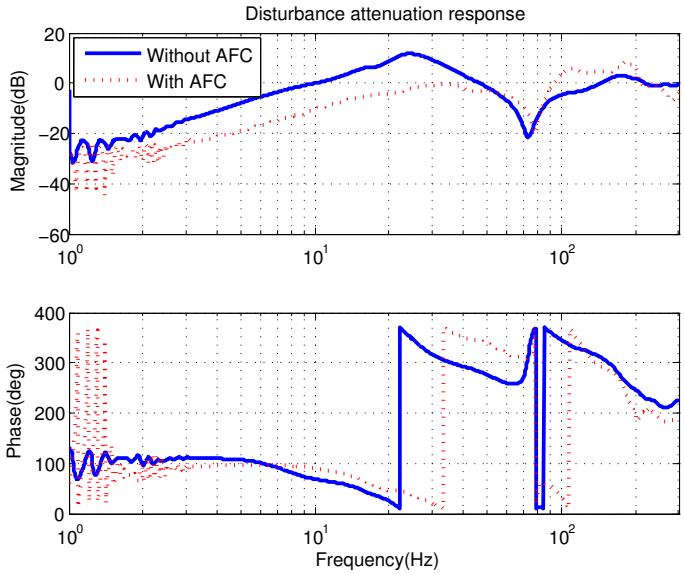

Fig. 6 Disturbance attenuation frequency response.

tion of the closed-loop current from $i_{\rm out}$ to $i_{\rm in}$ is shown below

$$\frac{i_{\rm out}}{i_{\rm in}} = \frac{G_{i1}G_1}{1+G_{i1}G_1}. \tag{10}$$

From Equation (10), maximizing the closed-loop bandwidth of the current to the master motor can offer a sufficient phase margin to the outer acceleration feedback loop.

3.2 Acceleration Loop

An angular acceleration sensor with high bandwidth is usually expensive. Two linear accelerometers (Han et al. 2007; Xu et al. 2000) can effectively calculate the angular acceleration signal with high accuracy. The open-loop transfer function of the acceleration is depicted in Equation (11)

$$G_{\rm Lo}(s) = \frac{\ddot{\theta}_L}{\tau} = \frac{K_1'}{J_L J_2' s^2 + (J_{\rm Lo}+2J_2')K_1'}. \tag{11}$$

The accelerometers do not sense the anti-resonance because they are mounted on the load side instead of the motor side. Therefore, such installation improves the closed-loop bandwidth of the acceleration. A cascade AFC (Han et al. 2007; Xu et al. 2000) instead of a plug-in AFC (Andersen & Zurbuchen 1976) is proposed for the control system. The acceleration controller is designed as

$$G_a(s) = \frac{K_a}{s(T_1 s^2 + T_2 s + 1)}. \tag{12}$$

The integrator makes the closed-loop response approximately constant at low frequencies while a second order

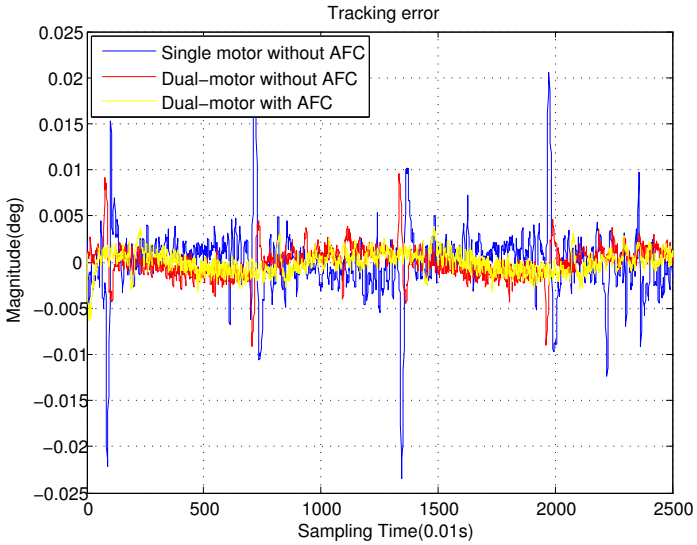

Fig. 7 Tracking error if the oscillatory motion is a sine wave.

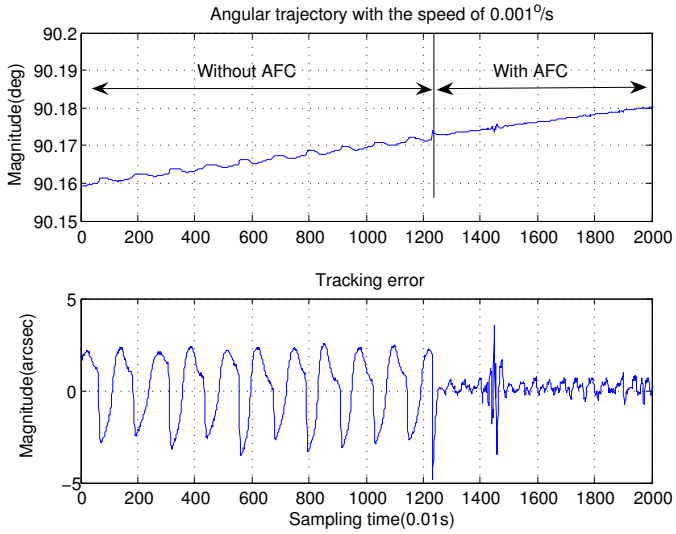

Fig. 8 The trajectory tracking with a speed of $0.001^\circ\ \mathrm{s}^{-1}$.

filter is used to attenuate the vibrations induced by mechanical resonances.

Comparing Figure 4 with Figure 2, the valley where the primary anti-resonance is located is not shown in the open-loop response of the acceleration in Figure 3. With the proposed acceleration controller, the bandwidth of the closed-loop response is more than 50 Hz.

3.3 Velocity Loop

Once the acceleration loop is closed, a classic PI-type controller is available for use as a velocity controller without the need for a notch filter.

The velocity-loop bandwidth with AFC is a little higher than that without an AFC, as shown in Figure 5. The main reason for this is attributable to the high acceleration-loop bandwidth. The peak value induced by mechanical resonances is attenuated by the AFC.

4 EXPERIMENTAL VERIFICATIONS

The frequency response of the disturbance attenuation is shown in Figure 6. With AFC, the attenuation at low frequencies is reduced by a factor of approximately -10 db (equivalent to three times), and the bandwidth of the disturbance attenuation is improved to 30 Hz, which is below the closed-loop bandwidth of the acceleration.

A 24-bit encoder is employed to generate a position closed loop.

Figure 7 compares the tracking errors of three systems (single motor without AFC, and dual motor without and with AFC). The oscillatory motion can be described by $60\sin(0.5t)$. The sampling time is 0.01 s. The control sys-

tem with a dual-motor drive either with AFC or without AFC has better performance than that with a single motor. It is very obvious that the peak error is almost eliminated by AFC.

In the dual-motor configuration, low speed tracking is experimentally verified in Figure 8 when the target speed is $0.001^\circ\,\mathrm{s}^{-1}$. The control system with AFC obtains a maximum position error of about $0.5''$, which is one fourth less than $2.0''$ without AFC.

These experimental results show that the proposed control method is effective either in high speed tracking or in low speed tracking. They also imply that the master-slave current control is well suited for synchronizing the two motors in the direct drive control mode.

5 CONCLUSIONS

The dual-motor drive configuration is employed to control the telescope's elevation axis by means of master-slave current control and acceleration feedback control. This configuration is beneficial to reduce the mechanical deformation of the connecting axis compared with the single motor system, and it may serve as an effective method to enhance closed-loop performance. Experiments were carried out to compare with the classical control mode. It has been shown through these experiments that the synchronized control mode with acceleration feedback control, due to high bandwidth of the closed-loop acceleration response, can help to attenuate mechanical resonances, improve control accuracy in low velocity tracking and suppress disturbance.

Acknowledgements The authors thank anonymous reviewers for their valuable comments, and also give thanks to the Youth Innovation Promotion Association, Chinese Academy of Sciences.

Appendix A: NOTATIONS

J_1, moment of inertia of the left motor
τ_1, output torque of the left motor
$\theta_1, \dot{\theta}_1, \ddot{\theta}_1$, angular displacement, velocity and acceleration of the left motor respectively
K_1, stiffness of the axis connecting the left motor and load
J_2, moment of inertia of the right motor
τ_2, output torque of the right motor
$\theta_2, \dot{\theta}_2, \ddot{\theta}_2$, angular displacement, velocity and acceleration of the right motor respectively
K_2 stiffness of the axis connecting the right motor and load
J_L, inertial moment of the load
$\theta_{\mathrm{Lo}}, \dot{\theta}_{\mathrm{Lo}}, \ddot{\theta}_{\mathrm{Lo}}$, angular displacement, velocity and acceleration of the load respectively
G_{p} (s), G_{v} (s), G_{a} (s), position, velocity and acceleration controller respectively
G_{i1} (s), G_{i2} (s) current controllers
G_{Lo} (s) Control plant (load)

References

Andersen, T., & Zurbuchen, R. 1976, ESO Tech. Rep., No. 7, 32 pp., 7

Ding, D.-W., Du, X., & Li, X. 2015, Automatic Control, IEEE Transactions on, 60, 1624

Ding, D.-W., Li, X.-J., Du, X., & Xie, X. 2016, IEEE Transactions on Fuzzy Systems

Gawronski, W. 2007, Control Systems Technology, IEEE Transactions on, 15, 276

Han, J. D., He, Y. Q., & Xu, W. L. 2007, Mechatronics, 17, 524

Higginson, A., Sanders, S., & Wallett, C. 1991, Mechatronics, 1, 509

MacMartin, D. G. 2003, in Proc. SPIE, Vol. 5054, Smart Structures and Materials 2003: Industrial and Commercial Applications of Smart Structures Technologies, ed. E. H. Anderson, 275

Perez-Pinal, F. J., Nuñez, C., Alvarez, R., & Cervantes, I. 2004, in Industrial Electronics Society, 2004. IECON 2004. 30th Annual Conference of IEEE, 2, IEEE, 1670

Pérez-Pinal, F. J., Nűňez, C., & Álvarez, R. 2005, in Electric Machines and Drives, 2005 IEEE International Conference on, IEEE, 1542

Rao, C., Gu, N., Zhu, L., et al. 2014, in Proc. SPIE, 9145, Ground-based and Airborne Telescopes V, 914529

Sedghi, B., Bauvir, B., & Dimmler, M. 2008, in SPIE Astronomical Telescopes+ Instrumentation, International Society for Optics and Photonics, 70121Q

Xu, W. L., Han, J. D., Tso, S. K., & Wang, Y. C. 2000, Industrial Electronics, IEEE Transactions on, 47, 150